

DOE/ER/3072-55
October 27, 1989

**PROPOSAL FOR AN EXPERIMENTAL STUDY OF
NONLINEAR COMPTON SCATTERING**

R.C. FERNOW, H.G. KIRK, and J. ROGERS
Brookhaven National Laboratory

I.J. BIGIO, N.A. KURNIT, and T. SHIMADA
Los Alamos National Laboratory

K.T. McDONALD,[†] D.P. RUSSELL, and M.E. WALL
Princeton University

Submitted to the Center for Accelerator Physics, Brookhaven National Laboratory

[†] Spokesperson

Summary

We propose to investigate nonlinear Compton scattering as the first experiment in a program to study the nonlinear quantum electrodynamics of electrons and photons in an intense electromagnetic wave. A laser beam of 10- μm wavelength, 6-picosecond (FWHM) pulse duration, and peak intensity $> 10^{15}$ Watts/cm² will be brought into head-on collision with a single bunch of 50-MeV electrons at the Brookhaven Accelerator Test Facility. At such intensities it is probable that an electron absorbs several laser photons before emitting a single photon of higher energy. In addition, the transverse oscillations of an electron inside the laser beam are relativistic, which leads to a shift in the effective mass of the electron that is discernible in the spectrum of radiated photons.

In the laboratory the laser beam is backscattered into x-rays. The peak brightness of the resulting beam of x-rays will exceed that available at any existing source, although the pulse repetition rate will only be a few per second. An x-ray spectrometer based on Bragg scattering off a graphite mosaic crystal will analyze the scattered light. Data collection and calibrations for the experiment should take about 200 hours. The observation of x-ray production via *e*-laser collisions will, we believe, be an essential diagnostic as to the successful synchronization of the laser and linac beams for any purpose.

Table of Contents

| | |
|--|----|
| 1. Theoretical Context | 1 |
| 2. Overview of the Experiment | 3 |
| 3. The Electron Beam | 6 |
| 4. The Laser System | 7 |
| 5. The Interaction Region | 7 |
| 6. The Electron Spectrometer | 9 |
| 7. The X-Ray Spectrometer | 10 |
| 8. Backgrounds | 15 |
| 9. Data Collection | 16 |
| 10. Costs | 17 |
| Appendices: | |
| A. The Ponderomotive Force | 18 |
| B. Attenuation of the Electron Beam by Compton Scattering | 19 |
| C. Anomalous Compton Scattering | 21 |
| D. Interference in Nonlinear Compton Scattering with Two Laser Beams | 23 |
| References | 23 |

1. Theoretical Context.

In the proposed experiment we wish to explore the simplest nonlinear interaction of a free electron with an intense electromagnetic wave. This work will serve as the starting point of an extended program of study of nonlinear quantum electrodynamics, as outlined in some detail in reference 1.

In the present experiment a 50-MeV electron beam is brought into head-on collision with a 10- μm -wavelength laser beam. The latter is so intense that an electron absorbs several laser photons before it emits a photon that carries away the sum of the energies of the absorbed photons. In the rest frame of the electron beam the laser photons have 20-eV energy, so the scattering process is well described in the classical limit (*i.e.*, Thomson scattering). In the laboratory frame, the final-state photons have keV energies, and the effect of multiphoton absorption may then be termed nonlinear Compton scattering.

In classical language, the criterion for the onset of nonlinear effects is that the transverse motion of the electron induced by the laser beam be relativistic. A useful measure of this is the field-strength parameter η , defined by

$$\eta \equiv \frac{eE_{\text{r.m.s.}}}{m\omega c} = \gamma_{\perp}\beta_{\perp},$$

where $\gamma_{\perp} = 1/\sqrt{1 - \beta_{\perp}^2}$, $\beta_{\perp} = v_{\perp}/c$, v_{\perp} is the transverse velocity of the electron, and $E_{\text{r.m.s.}}$ and ω are the root-mean-square electric-field strength and the angular frequency of the laser beam. For electrons in a wave with $\eta \gtrsim 1$ the magnitude of the radiation of the oscillating quadrupole (or higher) moment is comparable to dipole radiation. Of course, the higher multipole radiation occurs at higher harmonics of the oscillation frequency, which is equivalent to the earlier description that several photons are absorbed from the wave before a higher energy photon is emitted.

In plasma physics the quantity $eE/m\omega c$ is often called v_{osc}/c . As we are particularly interested in the regime where the value of this quantity exceeds 1, we adopt the new notation, η .

It is useful to record some numerical relations between η , the electric-field strength E , and the wave intensity I . First note that

$$I [\text{Watts/cm}^2] = \frac{\langle E^2 \rangle}{377 [\text{ohms}]} \quad \text{for } E \text{ in V/cm.}$$

Hence

$$E_{\text{r.m.s.}} [\text{V/cm}] = 19.4 \sqrt{I [\text{Watts/cm}^2]}.$$

Then we find

$$\eta^2 = 3.7 \times 10^{-19} I \lambda^2 \quad \text{for } I \text{ in Watts/cm}^2 \text{ and } \lambda \text{ in } \mu\text{m}.$$

For example, with $\lambda = 10 \mu\text{m}$ ($\hbar\omega = 0.124 \text{ eV}$), as in the proposed experiment, $\eta = 1$ corresponds to intensity $I = 2.7 \times 10^{16} \text{ Watts/cm}^2$, and in turn to an electric field strength of $E = 3 \times 10^9 \text{ V/cm}$.

At the focus of a diffraction-limited laser beam the intensity is related to the beam power by $I \approx \pi P / (2(f/d)^2 \lambda^2)$, where f/d is the ratio of the focal length to the aperture of the lens, so we have the approximate result

$$\eta^2 \approx \frac{57 \cdot P[\text{TeraWatts}]}{(f/d)^2},$$

independent of the laser wavelength.

A classical calculation of the radiation was first given by Schott² in 1912, which can be shown to be the correct limit of a quantum-mechanical calculation for nonlinear Compton scattering.³ Figure 1 shows the results of such a calculation for a 50-MeV electron placed in a plane wave of 10- μm wavelength and field-strength parameter $\eta = 0.3$. The Doppler shift gives dipole-radiation photons of energies up to 4.7 keV. Higher multipole radiation leads to the shoulders at higher photon energies seen in the figure.

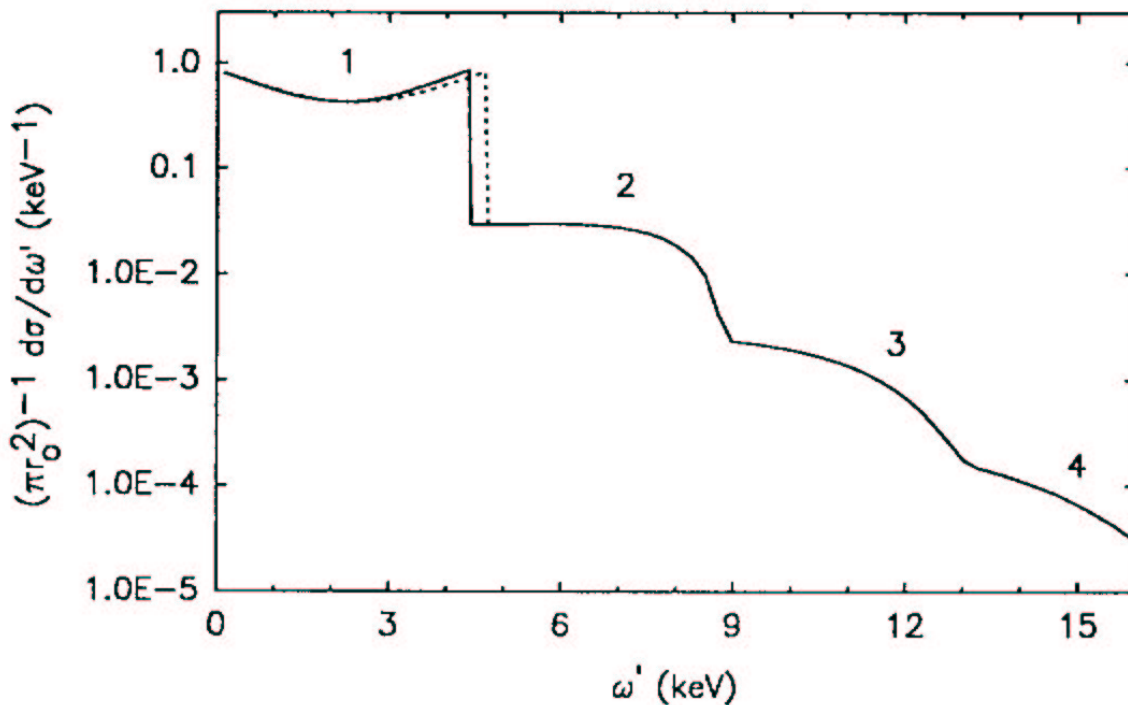


Figure 1. The differential cross section for nonlinear Compton scattering of a 50-MeV electron beam in head-on collision with a plane electromagnetic wave of 10- μm wavelength and field-strength parameter $\eta = 0.3$, as a function of the energy $\hbar\omega'$ of the scattered photons. The contributions due to absorption of 1 through 4 wave photons are labeled. The dashed curve is the ordinary Compton cross section. Note the shift in the end point of the one-photon energy spectrum for the case that $\eta = 0.3$.

An important effect related to the relativistic transverse motion of the electrons is the shift in the endpoint energy of the dipole-radiation spectrum, also seen in Figure 1. This arises in the Doppler-shift calculation because the boost to the (average) rest frame of the electron must take into account the transverse energy of the electron. This behavior can be summarized by saying that an electron in an intense wave field

has an effective mass

$$\bar{m} = m\sqrt{1 + \eta^2}.$$

Thus the endpoint energy, $\hbar\omega'_{\max}$, of the spectrum of the n^{th} -harmonic radiation is

$$\hbar\omega'_{\max} = \frac{4nU^2 \hbar\omega}{\bar{m}^2 c^4 + 4nU \hbar\omega},$$

where ω is the frequency of the laser and U is the electron energy. The ‘mass-shift’ effect on the energy spectrum will be a useful signature that the electron beam has actually passed through an intense-field region of the laser beam.

In Appendices A and B we discuss and dismiss the possibility that the laser beam might be so intense that the electrons cannot probe its high-field core. In Appendices C and D we consider two phenomena related to nonlinear Compton scattering, anomalous Compton scattering, and interference effects in nonlinear Compton scattering with two laser beams, that might be developed into followup experiments.

The experiment proposed here will observe the essential features of nonlinear Compton scattering: the higher harmonic components of the scattered light, and the mass-shift effect on the endpoint of the dipole-radiation spectrum. There has been only one previous experimental study of this subject,⁴ in which the η of the laser field was 0.01. This permitted detection of a very weak component of second-harmonic radiation, but did not allow any verification of the mass-shift effect.

2. Overview of the Experiment.

The experimental configuration is sketched in Figure 2. Some parameters of the electron-laser interaction region are summarized in Table 1.

The 50-MeV electron beam will be produced by the Brookhaven Accelerator Test Facility (ATF), whose rather small geometric emittance, $1.5(\pi) \times 10^{-9}$ rad-m (for a pulse of 10^7 electrons) permits the electron beam to be focused to a spot of radius $1 \mu\text{m}$ with a depth of focus $\beta^* = 0.67$ mm.[†] The laser beam is brought into head-on collision with the electrons by an off-axis parabolic mirror with $f/d = 2$. Figure 2 sketches the concept and Figure 3 shows a possible physical implementation. A hole of ~ 2 -mm diameter in the mirror lets the electron beam and the backscattered photons pass through. The unscattered laser beam will be collected in a second mirror and reflected out of the electrons’ path into a beam-flux monitor. The electrons are deflected by 20° in a dipole magnet 0.35 m downstream of the collision point, and their momentum spectrum is recorded by the beam-profile monitor. Photons that are backscattered to within 10 mrad of the electron-beam direction are analyzed in an x-ray spectrometer located 0.8 m downstream of the collision point.

For an estimate of the scattering rate we suppose the electron bunch has a pulse width of 2 ps (FWHM) and the laser pulse has a FWHM of 6 ps. The laser beam

[†] The depth of focus is the distance from the focal plane at which the spot size has grown by a factor of 2 in area. In accelerator argot, this is called the β^* , while in laser lingo it is called the Rayleigh range, z_R , or one-half the confocal parameter.

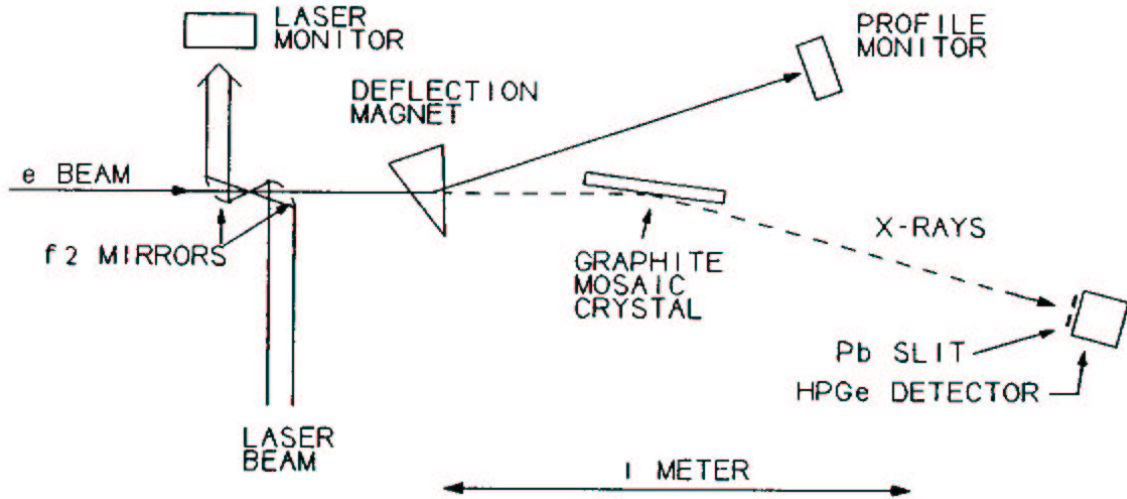


Figure 2. Layout of the proposed experiment.

Table 1. Parameters of the Compton Interaction Region

| Electron beam: | |
|---------------------------|--------------------|
| $\sigma_{r,e}$ | $1 \mu\text{m}$ |
| $\sigma_{\theta,e}$ | 1.5 mrad |
| β^* | 0.67 mm |
| Laser beam: | |
| λ | $10 \mu\text{m}$ |
| $\sigma_{r,\text{laser}}$ | $7 \mu\text{m}$ |
| z_R | $50 \mu\text{m}$ |
| Pulse length (FWHM) | 6 psec |
| η_{max} | 0.3 |

has total energy of 0.05 Joule. The electron and photon beams are taken to have Gaussian radial intensity profiles, with $\sigma_{r,e} = 1 \mu\text{m}$, and $\sigma_{r,\text{laser}} = 7 \mu\text{m}$ when the laser beam is focused by the $f2$ mirror. The confocal parameter for the laser beam is $100 \mu\text{m}$, less than 10% of the equivalent parameter, $2\beta^*$ for the electron beam. Hence the electron beam is essentially a uniform, small cylinder within the region where the laser intensity is high. The above variations of electron and photon flux over the interaction volume are then combined with the cross section (for circularly polarized laser light) to give the scattering rate.

Figure 4 summarizes the spectrum of scattered photons, calculated according to ref. 3. The total scattering rate is 0.05 per beam electron. Thus the probability that an electron scatters twice while crossing the laser beam is 0.0025. This places an important constraint on the x-ray detector, that it be able to tell a double scatter at the first harmonic from the rarer case of a single scatter at the second harmonic.

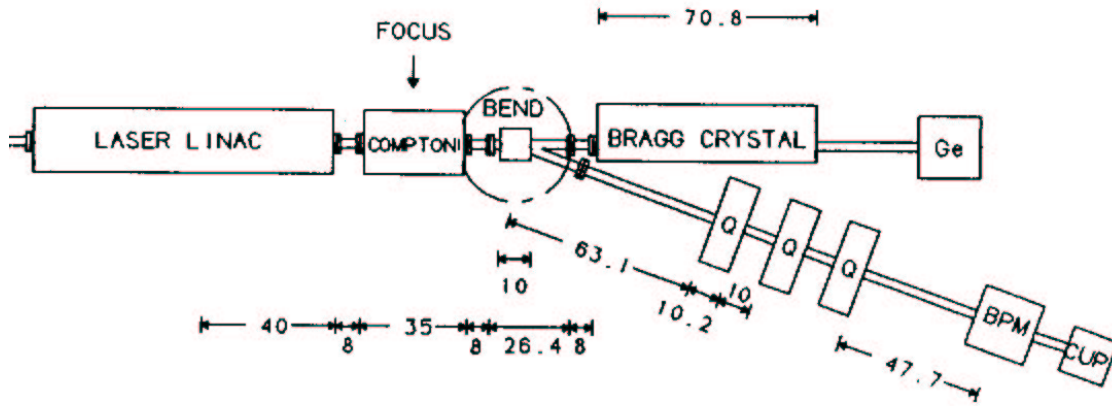


Figure 3. Proposed layout of electron spectrometer beamline including components of the Compton and LASER-LINAC⁶ experiments. The Compton interaction region is at the point labelled FOCUS inside the COMPTON vacuum chamber. The electrons are deflected downward by the BEND magnet and imaged by a quadrupole triplet onto a beam-profile monitor (BPM) or a Faraday CUP. The backscattered x-rays enter the BRAGG CRYSTAL vacuum housing and are scattered onto a germanium detector (Ge).

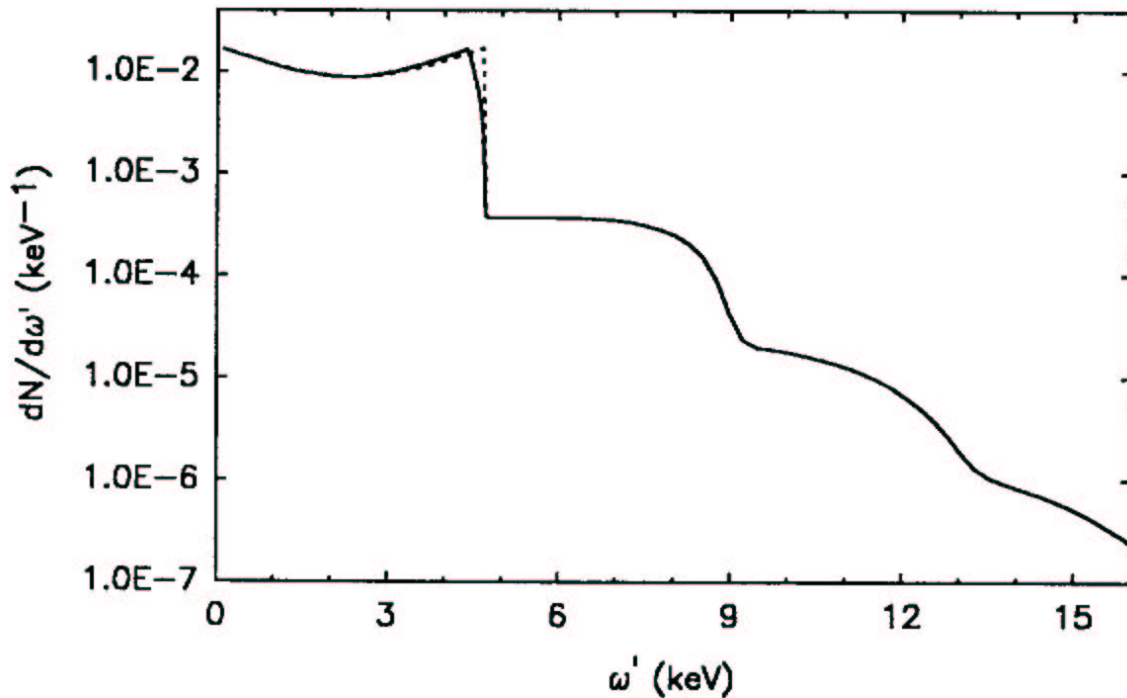


Figure 4. The scattering rate for a single 50-MeV electron in head-on collision with a laser beam of wavelength $10 \mu\text{m}$. The laser pulse has 0.05-Joule energy and 6-ps pulse length, and is focused in an $f/2$ mirror to achieve peak field-intensity parameter $\eta = 0.3$. The total scattering rate is 0.05 per electron. The dashed curve is the rate for Compton scattering if nonlinear effects are ignored.

The detector will not be able to resolve multiple photons in time during the 6-ps pulse, but must deflect x-rays of different energies by different angles so they can be separately counted. This is provided by a detector based on Bragg scattering off a graphite crystal, as discussed in Section 7.

Because the intensity of the laser beam is nonuniform near the focus the endpoint of the dipole-scattering spectrum is not sharp. Most of the scattering occurs in the high-field region, leading to the peak at 4.3 keV, while the rarer scattering in the low-field region populates the x-ray spectrum up to the unshifted endpoint of 4.7 keV. Despite this, the mass-shift effect will be clearly discernible in the data. In addition, the range in angle of incidence of the laser photons caused by the hard focusing leads to a downward shift of the Compton endpoint. However this shift is only about 1% for $f/d = 2$.

In the following sections we discuss briefly the electron beam, the laser system, the e -laser interaction region, the spectrometer to monitor the electron beam, the x-ray spectrometer, backgrounds, and the scenario for data collection.

3. The Electron Beam.

Table 2. Accelerator Test Facility Specifications

| Parameter | |
|---|----------------------------|
| Electrons per bunch | $\sim 10^7$ |
| Beam energy | 50 MeV |
| Repetition rate | ~ 1 pps |
| Electron energy spread $\Delta E/E$ (FWHM) | $\sim 0.1\%$ |
| Electron-bunch pulse length (FWHM) | 2 ps |
| Geometric transverse emittance at experiment | 1.5×10^{-9} rad-m |

Some basic parameters of the Accelerator Test Facility, as operated for the present experiment, are summarized in Table 2. The 50-MeV beam is accelerated in two SLAC-type cavities powered by a single klystron. The addition of a second klystron could increase the beam energy to 100 MeV. For a pulse of 10^7 electrons, a transverse geometrical emittance (at the final focus) of 1.5×10^{-9} rad-m is to be achieved by a very small illumination (200- μ m radius) of the photocathode of the electron gun, and by the small transverse energy (1.5 eV) of the electrons ejected from the Yttrium photocathode.⁵

The electron beam is brought from the linac to the experiment in a beam transport which permits a final focus of about 1- μ m radius. The corresponding beam divergence is 1.5 mrad, and the depth of focus is $\beta^* = 0.67$ mm. Emittance-defining collimators along the beam transport will allow cleanup of the beam and further reduction of the emittance, if desired. Using the momentum-analysis section of the beam transport, the beam energy spread could be collimated to 0.01%, with a loss in beam intensity.

The linac structure and any collimators in the beam transport are a likely a source of x-rays, which will be the principal source of background for the experiment. This background will be greatly reduced by the dog-leg bend in the beamline, but lead shielding around the experiment will likely be required.

4. The Laser System.

The laser system for the present experiment is the same as that being developed at Los Alamos National Lab for the laser-grating-accelerator experiment.⁶ In principle, either the Nd:YAG laser front end⁷ (1- μm wavelength) or the CO₂ amplifier⁸ (10- μm wavelength) could be improved to achieve the desired field-strength of $\eta = 0.3$ or higher. Effort devoted to obtaining higher power pulses at 10- μm wavelength will pay off in the enhanced performance of the Accelerator Test Facility as an x-ray source, and is considered in the present proposal. An alternative scheme based on upgrading the 1- μm -wavelength front end of the laser is considered in ref. 1.

A block diagram of the laser system and its interconnection with the electron linac is shown in Figure 5. Both the laser and the linac derive their timing reference signals from a highly stable reference oscillator. The laser front end is a mode-locked cw Nd:YAG oscillator which is also phase locked to the reference oscillator via a feedback loop.⁹ A few pulses per second from the Nd:YAG oscillator are amplified and compressed.⁷ These serve to trim the long output pulses of the hybrid CO₂ oscillator⁸ into pulses of 6-ps duration.¹⁰ The short CO₂ pulses are then amplified to energy greater than 0.05 Joule in a multipass gain module filled with a mix of CO₂ isotopes. If desired, an additional gain module could be added to achieve extremely high pulse energies.

The picosecond CO₂ pulses have an energy spread of around 2%. Thus the end-point energy of the first-harmonic Compton spectrum is blurred by this amount. As the mass-shift effect is $\sim 10\%$, it should not be obscured by this blurring.

The interpretation of the nonlinear Compton scattering is somewhat cleaner if circularly polarized laser light is used. The laser system delivers linearly polarized light via Brewster-angle windows on the CO₂ amplifier. Circularly polarized light can be obtained by use of a quarter-wave plate. Some data will be collected with linearly polarized light as a check.

5. The Interaction Region.

The laser beam is brought to a focus in a head-on collision at the final focus of the electron beam. Some parameters of the focal region relevant to nonlinear Compton scattering are summarized in Table 1 and discussed in Section 2. Here we consider mechanical aspects of the interaction region.

The power level of the laser beam is 10 GW, which favors the use of reflection optics. An off-axis parabolic mirror of $f/d = 2$ will focus the laser beam, which will be nearly parallel as it enters the interaction-region vacuum chamber through a 5-cm-diameter ZnSe window. The mirror diameter will also be 5 cm, and hence will be located 10 cm from the *e*-laser interaction point. At this distance the electron

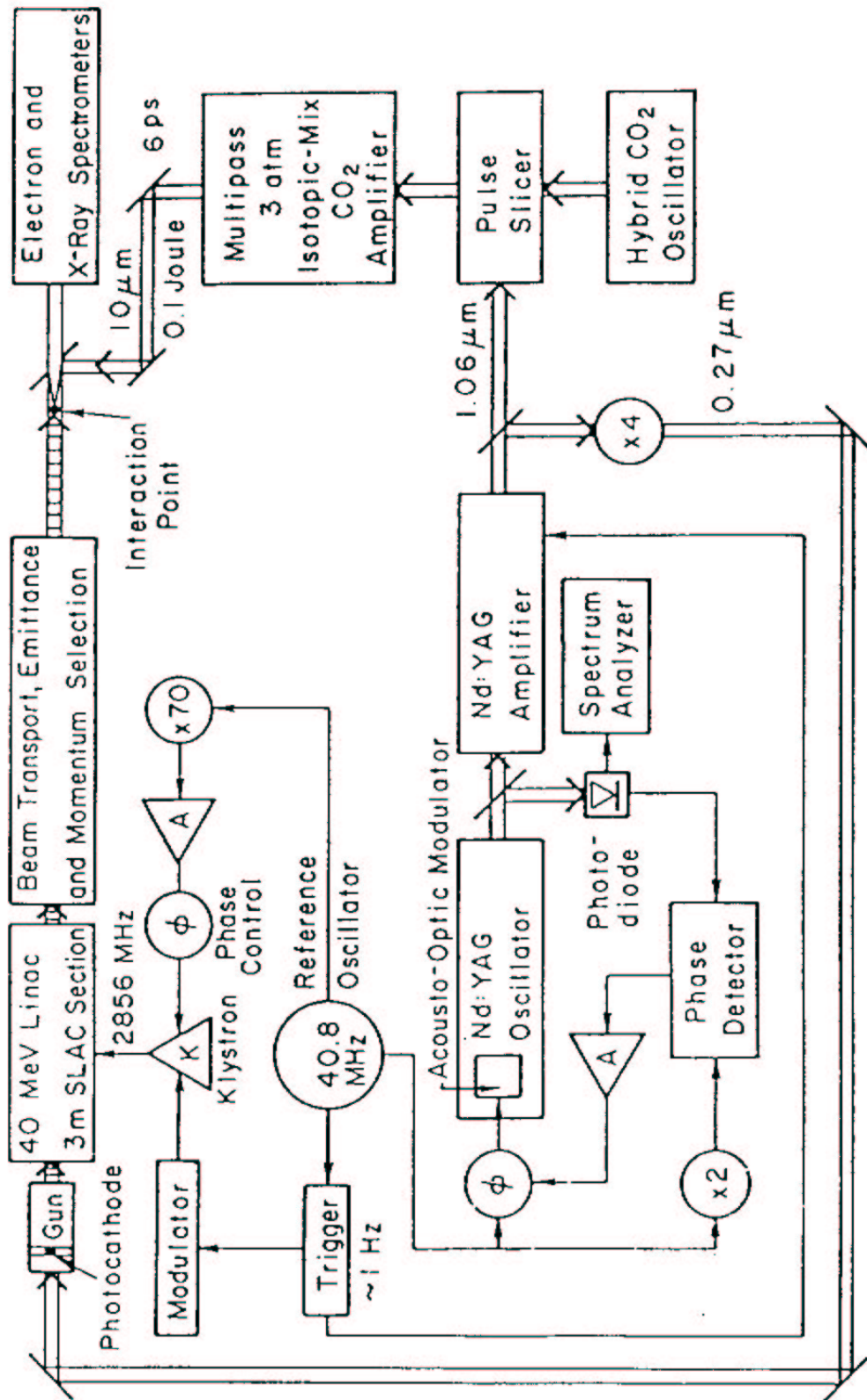


Figure 5. Block diagram of the laser system and its synchronization with the electron linac.

beam radius is $150\ \mu\text{m}$ r.m.s. The electron beam will pass through a 2-mm-diameter hole in the mirror, as sketched in Figures 2 and 3.

The unscattered laser beam will be collected in a second parabolic mirror, and brought to a beam-flux monitor. The two mirrors will be mounted together on an x - y translation stage capable of $0.1\text{-}\mu\text{m}$ steps, such as manufactured by Aerotech. Transverse alignment of the laser beam onto the electron beam will be accomplished via these motions, while longitudinal alignment is performed by changing the quadrupole strengths in the final focus of the electron beamline. Temporal synchronization is attained via an optical delay line in the CO_2 beam transport. The x-ray detector (section 7) will serve as a monitor of the rate of electron-photon collisions during the beam alignment.

The interaction region will be maintained at a vacuum of 10^{-5} - 10^{-6} torr. The drive motors for the translation stage could be located inside the vacuum chamber while maintaining a vacuum of 10^{-6} torr. The vacuum chamber will be placed just downstream of the laser-grating experiment so that either experiment could be activated by placing the electron-beam focus at the chosen interaction region. The focusing mirrors for the present experiment can be moved completely out of the electron beamline during the grating-accelerator experiments.

6. The Electron Spectrometer.

After the electron beam passes the interaction point, it must be deflected to one side to allow the scattered photons to be analyzed. The magnet required for this also serves as the dispersive element in a precision electron spectrometer, sketched in Figures 2 and 3. The dipole magnet has a field of 5.8 kGauss, a field integral of 0.058 Tesla-m (for the 50-MeV beam), and deflects the electrons by 20° . The electron beam then impinges on a beam-profile monitor with $\sim 50\text{-}\mu\text{m}$ resolution,¹¹ located 1 m downstream of the deflection magnet. The spectrometer will be capable of 10-keV resolution for the 50-MeV electrons. A Faraday cup downstream of the profile monitor will serve as the primary electron-beam-flux monitor, measuring the beam intensity as a function of momentum.

While the electron spectrometer is not as critical to this experiment as to the laser-grating experiment,⁶ the spectrometer beamline (Figure 3) has been designed to retain the essential features required by the laser-grating while accommodating the geometric constraints of the Compton experiment. For example, it is necessary to minimize the distance from Compton interaction point to x-ray spectrometer, which is placed in the undeflected continuation of the beamline after the dispersion magnet. For this reason the quadrupole triplet is placed after the dipole, in the deflected beamline. Due to the imaging requirements of the laser-grating experiment, the deflection will be vertical (downward).

The design parameters of the beam transport of the electron spectrometer are summarized in Table 3.

Table 3. Electron Spectrometer Specifications

| | |
|---|-----------------|
| Laser-linac focus to dipole entrance | 100 cm |
| Path length in dipole | 10 cm |
| Dipole field | 5.8 kGauss |
| Bend angle | 20° |
| Dipole exit to 1st quadrupole in triplet | 63 cm |
| Quadrupole effective length | 10.2 cm |
| Drift length between quadrupoles | 10 cm |
| Outer quadrupole field strengths | -0.26 kGauss/cm |
| Inner quadrupole field strength | 0.55 kGauss/cm |
| Third quadrupole exit to beam-profile monitor | 47 cm |
| Horizontal dispersion at monitor | 2.8 mm/% |
| Vertical deflection (at laser-linac) dispersion | 2 mm/mrad |

7. The X-Ray Spectrometer.

As shown in Figure 4, laser photons that backscatter off the electron beam are Doppler-shifted to x-ray energies. During a 2-ps pulse of 10^7 electrons we expect 5×10^5 x-rays to be produced. To analyze these we need an x-ray spectrometer that disperses x-rays of different energies to different positions. Then a Germanium total-absorption detector that measures the total energy of x-rays arriving at a fixed position will determine the x-ray flux within a well-defined energy bin.

The nonlinear mass-shift effect (at the proposed laser intensity) reduces the endpoint of the x-ray spectrum by some 10% compared to weak-field Compton scattering. (See Figure 4.) Thus bins of 1% in x-ray energy would be quite suitable to analyze the effect. This is 10–100 times broader than the bandwidth of a typical x-ray monochromator that uses a perfect crystal. However, our requirements are well matched to the capability of a spectrometer based on a flat pyrolytic graphite crystal,¹² in which there is a spread (or mosaic) of 0.8° in the orientations of the planes of the microcrystals.

The simultaneous functioning of the graphite crystal as a dispersive and focusing element is sketched in Figures 6 and 7. We are fortunate in having a very good approximation to a point source at the electron-photon interaction region. This is shown at distance L from the center of the crystal, which is oriented at the Bragg angle θ_B for x-rays of energy E . An x-ray of energy E traveling along the central ray will penetrate into the crystal until it meets a microcrystal with its crystal planes at angle θ_B to the x-ray. The x-ray then scatters by angle $2\theta_B$ with about 40% efficiency.

Now consider an x-ray also of energy E , but which makes angle $\Delta/2$ to the central ray, as shown in Figure 6. If the graphite were in the form of a single perfect crystal, this x-ray would not strike the crystal planes at the Bragg angle θ_B , and would not be scattered. But if Δ is less than or equal to the mosaic spread of the graphite crystal then the x-ray does scatter off some microcrystal, again with scattering angle $2\theta_B$. The paths of the two scattered x-rays cross approximately at distance L from

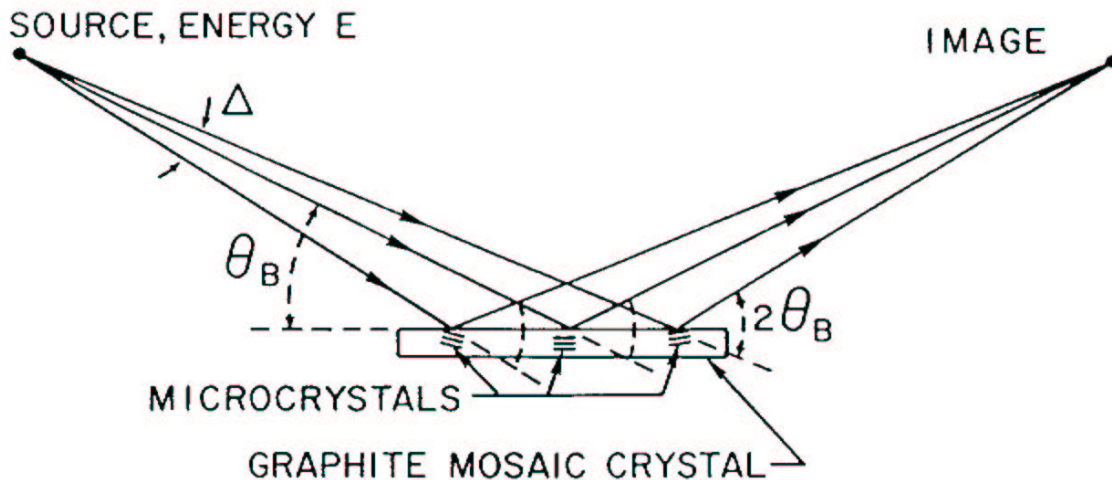


Figure 6. The scattering of monoenergetic x-rays by a graphite mosaic crystal. The scattering angle is always twice the Bragg angle θ_B . The mosaic spread, Δ , of orientations of the microcrystals results in a focusing geometry with angular acceptance Δ .

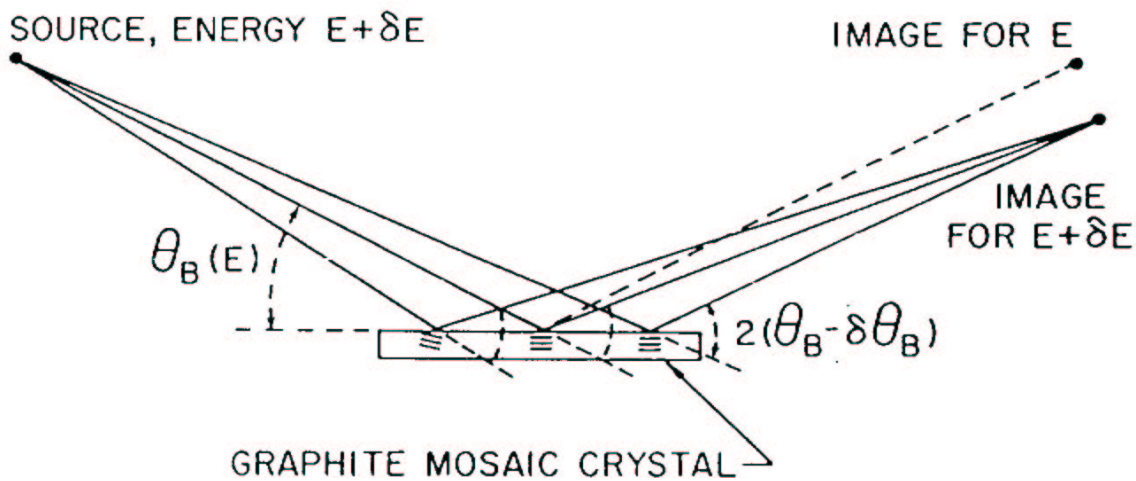


Figure 7. X-rays of energy $E + \delta E$ are focused by Bragg reflection off a graphite mosaic crystal to a different point than those of energy E .

the crystal. That is, the variable orientation of the microcrystals within the flat macrocrystal duplicates the focusing effect (in the scattering plane only) of a bent perfect crystal.

Next consider the case of x-rays with energy $E + \delta E$, as shown in Figure 7. The corresponding Bragg angle is now $\theta_B - \delta\theta_B$. Such an x-ray traveling along the central ray at angle θ_B to the crystal could not scatter off a perfect crystal. But if $\delta\theta_B < \Delta/2$, where from now one Δ is taken to mean the mosaic spread angle (FWHM) of the graphite crystal, the x-ray will find some microcrystal off which it can scatter, with scattering angle $2(\theta_B - \delta\theta_B)$. Similarly, x-rays of energy $E + \delta E$ that make small angles to the central ray also scatter off some microcrystal, and are brought to a focus at distance L from the crystal. Because of the dependence of the Bragg angle on x-ray energy, the scattered x-rays disperse along a focal plane as desired.

For numerical computation it is useful to note the Bragg relation for graphite:

$$\sin \theta_B = \frac{1.85}{E[\text{keV}]}.$$

This follows from the usual form of Bragg's law,

$$\sin \theta_B = \frac{\lambda}{2d},$$

the useful conversion formula

$$\lambda[\text{\AA}] = \frac{12.38}{E[\text{keV}]},$$

and the fact that the crystal-plane separation in graphite is $2d = 6.71 \text{ \AA}$. The dispersive effect can be calculated by taking the derivative of the Bragg law:

$$\cot \theta_B \delta\theta_B = \frac{\delta E}{E},$$

which is well approximated in graphite for $E \gtrsim 10 \text{ keV}$ by

$$\delta\theta_B = \frac{1.85}{E[\text{keV}]} \frac{\delta E}{E}.$$

For example, with $E = 4.7 \text{ keV}$, the Bragg angle is 400 mrad, so the scattering angle is 46° . For a 1% bite $\delta E/E$ about 5 keV, the angular bite is $\delta\theta_B = 4 \text{ mrad}$, considerably less than the mosaic spread angle, $\Delta = 0.8^\circ = 14 \text{ mrad}$, of a commercially available graphite crystal.

The distance L from the source to the crystal, and hence from crystal to the detector, is 0.8 m. Then a slit of width $L \cdot \delta\theta_B = 3.2 \text{ mm}$ at the face of the detector will define the 1% energy acceptance.

The angular acceptance (in the scattering plane) of the spectrometer is in principle limited only by the mosaic spread angle Δ of the graphite crystal. To maximize the angular range the crystal must have length

$$l = \frac{L \cdot \Delta}{\sin \theta_B} = \frac{L \cdot \Delta \cdot E[\text{keV}]}{1.85}.$$

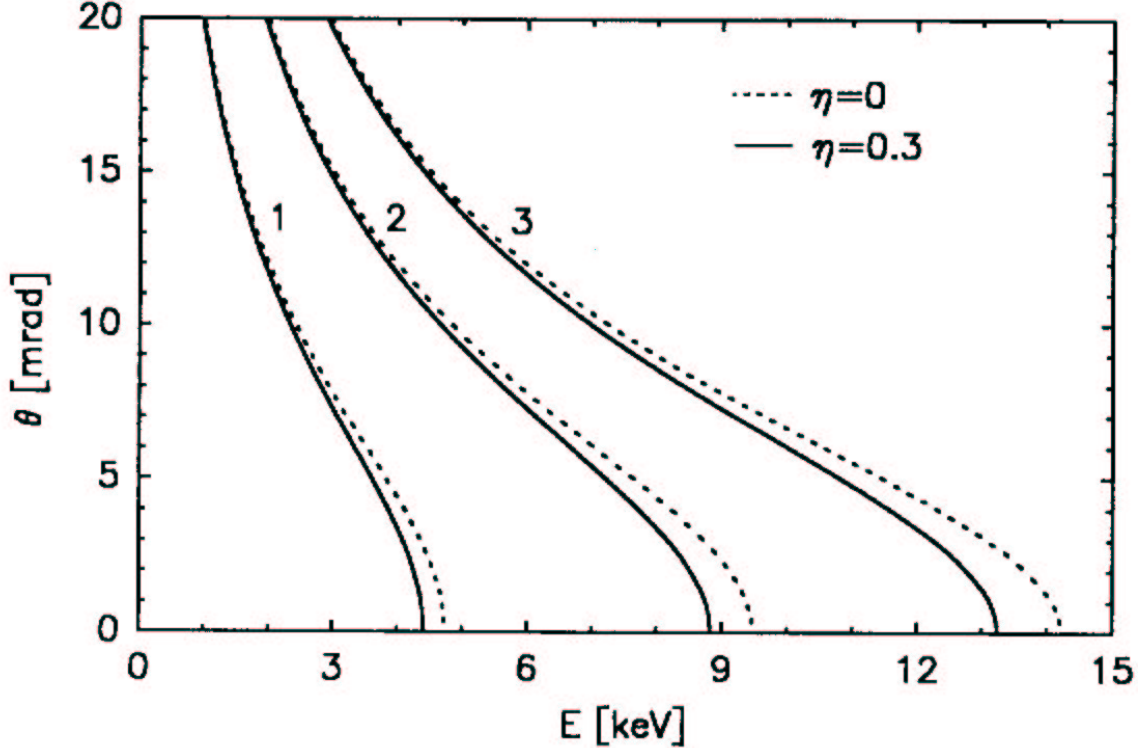


Figure 8. The relation between x-ray production angle and energy for the first three harmonics in nonlinear Compton scattering of 50-MeV electrons and a 10- μm laser beam. The bands are due to the intensity dependence of the nonlinear effects.

A longer crystal does not enhance the acceptance as the spread in mosaic angles is insufficient to direct the larger-incidence-angle x-rays onto the detector. In the present experiment we wish to analyze up to the third harmonic scattering for which $E \sim 13$ keV, which requires a crystal length $l \sim 8$ cm.

Another way to think about the the angular acceptance is illustrated in Figure 8, which shows the relation between x-ray energy and angle θ relative to the direction of the electron beam for the first three harmonics in nonlinear Compton scattering. Because the electron beam will pass through regions of various laser-beam intensities, there will be a range of x-ray energies produced at any fixed angle. The bands in Figure 8 show this range corresponding to field-strength parameter η between 0 and 0.3. The scattering rate will be much higher on the $\eta = 0.3$ edge of the bands. With a graphite crystal of mosaic spread angle $\Delta = 14$ mrad, there will be full collection efficiency out to production angle 7 mrad. The collection efficiency decreases at larger angles and will be determined experimentally by a calibration run utilizing the well-known spectrum of x-rays from linear Compton scattering (which requires a reduced laser intensity such that $\eta \ll 1$).

The flat-crystal geometry of the spectrometer does not provide any focusing transverse to the scattering plane. With source and detector equidistant from the crystal, the transverse size of the image on the detector is twice that of the intercept of the

x-rays at the crystal. We desire the transverse angular acceptance to match that in the scattering plane. Hence the transverse extent of the graphite crystal should be at least $L \cdot \delta\theta \approx L \cdot \Delta \approx 11$ mm, and that of the detector should be at least $2L \cdot \Delta$. However, there is an additional effect on the transverse size of the image on the detector. Due to the mosaic spread, Δ , of the microcrystals, the x-rays that scatter from a given point on the graphite crystal have a spread of angles, 2Δ , in azimuth. These x-rays then describe an arc of length $l = L \cdot 2\Delta \cdot \sin\theta_B$ over the face of the detector. To maintain good acceptance, the detector should thus have transverse extent of $2L \cdot \Delta \cdot (1 + \sin\theta_B) \approx 31$ mm in present case.

The commercial pyrolytic graphite crystals are available as disks of 8 cm in diameter. While a crystal longer than 8 cm in the scattering plane is of no use as mentioned above, a transverse size greater than 11 mm can yield partial acceptance for x-rays of production angle $\theta > \Delta/2 = 7$ mrad. For example, with $\theta = \Delta = 14$ mrad, a graphite-crystal width of 22 mm, and a detector width of $2L \cdot \Delta \cdot (2 + \sin\theta_B) \approx 54$ mm, full acceptance could be maintained over the 8-cm length of the graphite crystal, corresponding to 50% overall acceptance. This suggests the use of a 50- or 60-mm diameter Ge x-ray detector.

Several additional factors conspire to reduce the total efficiency of the x-ray spectrometer. While the x-rays of production angle out to 7 mrad are accepted with 100% efficiency by the detector geometry, they are attenuated by the passage through matter between production and detection. As already noted, x-rays scatter off the mosaic crystal with 40% efficiency. They must then pass out of the crystal vacuum housing through a beryllium window of approximate thickness 3 mils. The Ge detector has a 20-mil beryllium window through which x-rays must also pass. This combined thickness of beryllium will pass 40% of the 4-keV x-rays and over 90% of the 10-keV x-rays. If the crystal housing is constructed so as to minimize the air gap between the exit window and the Ge detector, then the ~ 2 -cm gap will pass about 90% of the 4-keV x-rays and essentially 100% of the 10-keV x-rays. Another possibility is to construct the crystal chamber to contain only the crystal and associated mechanics, leaving the remaining distance to the detector (~ 50 cm) in air. This would attenuate the 4-keV x-rays down to 4% and the 10-keV x-rays down to 75%.

Combining these effects, the total efficiency for 4-keV x-rays is 15% with a large crystal housing, 0.6% with a small housing. The efficiency for 10-keV x-rays is 35% with a large housing, 25% with a small housing. For the purposes of data-rate calculations, the larger efficiencies will be assumed. It is fortunate that the attenuation is least severe for x-rays of higher energy, where the Compton-scattering rate is low.

In summary, the configuration of the x-ray spectrometer is simple and classic. The graphite crystal is mounted on a rotating stage located 0.8 m from the *e*-laser interaction point, along the line of the electron beam (see Figure 3 for a side view, and Figure 9 for a top view). X-rays of a given energy are brought to a focus 0.8 m from the crystal, after scattering at twice the Bragg angle. A slit defines the width of the energy bin, and the number of x-rays in that bin is determined by measurement of the sum of their energies in a Ge solid-state detector, such as Ortec Model LO-

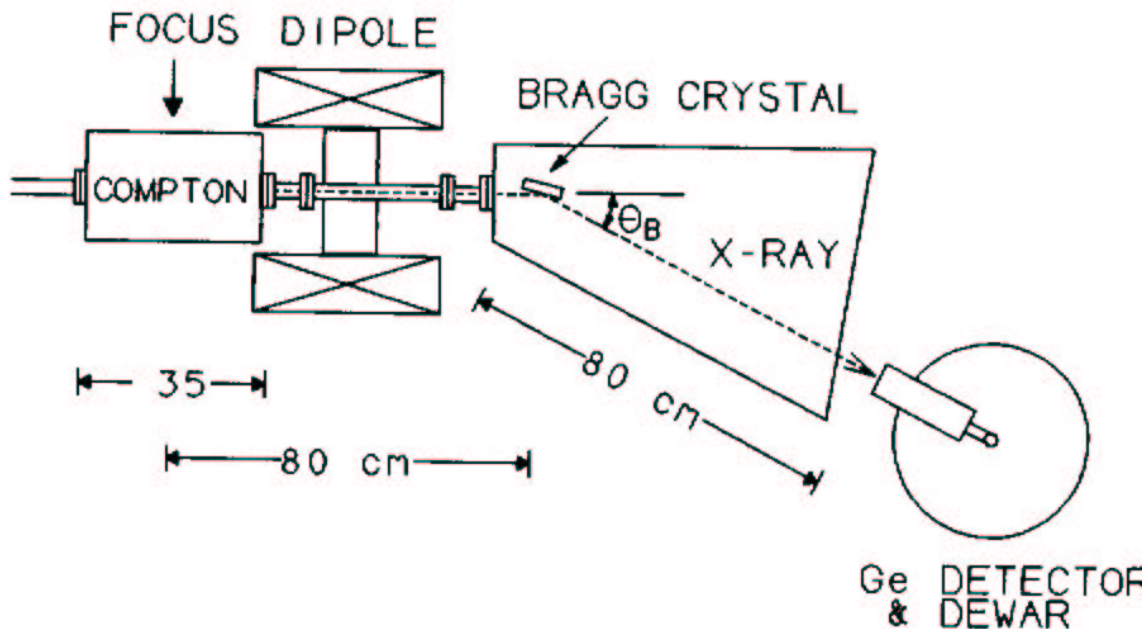


Figure 9. Top view of the Bragg scattering spectrometer.

AX-51370-20-P.

8. Backgrounds.

Background x-rays could arise from synchrotron radiation in the deflection magnet (and from the upstream beamline magnets), from bremsstrahlung of the electron beam off residual gas in the vacuum chamber, or from bremsstrahlung off the emittance-defining collimators in the beam line. The latter effect is likely to be the most serious, but is hard to estimate quantitatively. Considerable care will be required to install the necessary shielding against this source. We now show that the other two sources may be calculated to be negligible.

Concerning synchrotron radiation, recall that the characteristic frequency radiated by an electron of energy $U = \gamma mc^2$ in a magnetic field B is

$$\omega \sim \gamma^3 \omega_0 = \gamma^2 \frac{eB}{mc} = 511 \gamma^2 \frac{B}{B_{cr}} [\text{keV}],$$

where $B_{cr} = m^2 c^3 / e \hbar = 4.41 \times 10^{13}$ Gauss. Thus for $U = 50$ MeV and $B = 5800$ Gauss we find $\omega = 0.6$ eV, which is hardly in the x-ray range. Furthermore, the total energy radiated in one revolution is

$$\frac{\Delta U}{U} = \frac{4\pi}{3} \alpha \gamma^2 \frac{B}{B_{cr}}.$$

For a 20° bend and the above parameters for U and B , we have $\Delta U = 0.13$ eV, or 0.2 radiated photon per electron. Clearly there can be no significant tail into the keV region.

Concerning scattering off residual gas, suppose we have as much as 10-m path in a vacuum of 10^{-5} torr. Assuming the residual gas to be air, the radiation length at

this pressure is then 2×10^{10} m. For 10^7 electrons of 50-MeV energy traversing 10 m of this gas, the total radiated energy is about 250 keV. This energy is distributed according to the $1/U$ bremsstrahlung spectrum, and contributes only 1/4 keV to a 1% energy bin. Still, a vacuum of 10^{-6} torr would be preferable.

9. Data Collection.

The thermal limitations of the final laser amplifier may restrict the repetition rate of the experiment to less than 10 pulses per second. For the purpose of rate estimates we assume only one pulse per second.

The expected rate of x-ray production per electron is presented in Figure 4, for laser operation at design intensity. As noted in section 2, up to 10^7 electrons per pulse can be provided by the Accelerator Test Facility and focused into a volume smaller than that of the laser focus. With a total scattering probability of 0.05 per electron, some 5×10^5 x-rays will be produced each pulse. These are largely due to first harmonic scattering, which populates the 0–4.7 keV region of the x-ray spectrum. In a 1% energy bin (47 eV) we then expect about 5000 x-rays per pulse, of which about 750 would be detected, assuming an overall efficiency of 15% as estimated in Section 7. Statistical accuracy of 2% would be obtained with only 3 pulses.

For a pulse of 10^7 electrons, the electron-beam divergence is about 3.5 mrad (FWHM), which would smear the x-rays at the endpoint over 5 mm at the Ge detector located 1.6 m from the interaction region. As rate is no problem for the first-harmonic photons, but we desire to resolve the mass-shift effect, it would be advantageous to reduce the beam to 10^6 per pulse during studies of the first-harmonic scattering. This would reduce the smearing at the detector to 0.5 mm. Then some 30 pulses would be required per data point.

The graphite-mosaic-crystal spectrometer will collect x-rays only within about 10 mrad of the electron-beam direction. Referring to Figure 8, we see that we will be able to explore readily only the upper 30% of the energy range of each harmonic. That is, some 30 spectrometer settings of 1% bandwidth would constitute a data run at each harmonic.

According to Figure 4, the scattering rate at the third harmonic will be about 1/1000 that at the first harmonic, with detection efficiency of about 30%. Hence there would be about 1.5 third-harmonic x-rays per pulse of 10^7 electrons in a 1% bin, so that 2% statistical accuracy could be obtained in about 1800 pulses, or 1/2 hour of running. A scan of 30 spectrometer settings would then take 15 hours. Fourth-harmonic scattering would take an order of magnitude longer to study.

In section 7 we mentioned the need to calibrate the x-ray spectrometer on the ordinary Compton-scattering spectrum obtained with a low-intensity laser beam. To avoid any nonlinear mass-shift effect on the spectrum to the 1% level, the laser field-intensity parameter η^2 should be less than 0.01. (Recall from Section 1 that the position of the ‘Compton edge’ of the energy spectrum is multiplied by $\sim 1/(1 + \eta^2)$ in a strong field.) As the laser-photon flux is also proportional to η^2 , the scattering rate would then be 10 times smaller than that at the nominal operating condition

of $\eta = 0.3$. Thus in the calibration run, which can only explore the first harmonic scattering, there will be about 75 detected x-rays per pulse of 10^7 electrons in a 1% energy bin. To calibrate the spectrometer at energies above 4.7 keV, the electron beam energy will be raised. For example, 6-keV x-rays will be studied with 56-MeV electrons, and 9-keV x-rays with 70-MeV electrons, noting that the scattered x-ray energy varies as the square of the electron-beam energy. At each beam energy the calibration should take about one or two hours.

Thus once the apparatus is fully working, the entire data collection of first-through fourth-harmonic scattering could be performed in about 150 hours, with final calibration occupying an additional 10 hours. We request a run of 200 hours, allowing some safety factor.

10. Costs

Below we give a cost estimate for items to be provided by Princeton University for the nonlinear Compton scattering experiment. No additional funding is required for the CO₂ laser now being built by some of us at Los Alamos for the ATF. Also not shown is the cost to BNL for installation of the experiment, including such shielding as may be needed for the Ge detector.

| | |
|--|--------------|
| 1. X-ray Beam Diagnostic | \$50k |
| a. Ortec LO-AX-51370-20-P Ge detector and electronics | \$20k |
| b. $f2$ mirrors for the laser focus | \$5k |
| c. Vacuum chamber for the $f2$ mirrors | \$5k |
| d. Optical beam transport to the $f2$ mirror | \$5k |
| e. Remote position control for x , y and t scans | \$10k |
| f. PC-clone computer to control the diagnostic system | \$5k |
| 2. Nonlinear Compton Scattering Experiment | \$20k |
| a. Pyrolytic graphite crystal | \$5k |
| b. Movable Pb slit and positioner | \$5k |
| c. Vacuum chamber for the crystal spectrometer | \$10k |
| Total | \$70k |

The \$50k required for the ‘x-ray beam diagnostic’ has been already funded by the D.O.E. as part of Princeton’s contribution to the ATF itself.

Appendix A. The Ponderomotive Force

The fields of an intense, focused laser are so strong that an electron may be deflected by the laser before it reaches the core of the laser pulse. Here we examine the size of this effect as constrained by the laws of diffraction .

First recall the argument given in section 2-1d of ref. 1.

The effective mass, \bar{m} , of an electron inside a wave field can be thought of as associated with an effective potential:

$$U_{\text{eff}} = \bar{m}c^2 = mc^2 \sqrt{1 + \eta^2},$$

where $\eta^2 = e^2 \langle E^2 \rangle / (m\omega c)^2$ is the classical, dimensionless measure of the intensity of the electric field E .

For a field that is nonuniform, the intensity gradient can be associated with a force,

$$F = -\nabla U = -\frac{mc^2}{2\sqrt{1 + \eta^2}} \nabla \eta^2.$$

If the wave field is that of a focused laser beam, intensity gradients occur because of the laws of diffraction. This is usefully expressed by the shape of a Gaussian laser beam,

$$\eta^2(r, z) = \frac{\eta_0^2}{1 + z^2/z_R^2} \exp\left(\frac{-r^2}{2\sigma_r^2(1 + z^2/z_R^2)}\right),$$

where σ_r describes the transverse Gaussian intensity profile of the beam at its waist, and

$$z_R = \frac{4\pi\sigma_r^2}{\lambda}$$

is called the Rayleigh range and measures the length over which the intensity falls by 2 along z (assuming a sinusoidal time dependence).

The laser beam may also be pulsed. We suppose it to have a gaussian profile in time, and let σ_t be the corresponding variance.

Note that there are now two reasons for longitudinal intensity gradients: the Rayleigh range of diffraction, and the temporal pulse width. For a tightly focused laser beam, the Rayleigh range is likely to be shorter than the temporal pulse width, and hence dominates the longitudinal intensity gradient.

A focus is achieved with a lens (or mirror). If the laser beam is ‘matched’ to the lens in the sense that $\sigma_r(\text{lens}) = d/4$ where d is the diameter of the lens, then about 86% of the beam passes through the lens to be focused. In this case, the diffraction-limited spot size, σ_r , at the focus is given by

$$\sigma_r = \frac{\lambda f}{\pi d},$$

where f is the focal length of the lens. A good lens might have $f/d = 2$, leading to $\sigma_r = 2\lambda/\pi$ and $z_R = 16\lambda/\pi$. For σ_t to be less than z_R would require a pulse

of duration less than 5 cycles r.m.s, or 13 cycles full-width at half-maximum. This condition has been met only in very special low-power lasers.

Given that the laws of diffraction determine the intensity profile, we see that the transverse gradient is always larger than the longitudinal for any lens with $f/d > 1/4$. Thus the relevant form for $\nabla\eta^2$ is

$$\frac{d\eta^2}{dr} \text{ whose peak value is approximately } \frac{\eta_0^2}{\sigma_r}.$$

The corresponding transverse force lasts for a time approximately $z_R/c = 4\pi\sigma_r^2/\lambda c$, so the electron experiences a transverse momentum kick of

$$\Delta P_T \approx 2\pi mc \frac{\eta_0^2}{\sqrt{1+\eta_0^2}} \frac{\sigma_r}{\lambda}$$

on its way into the laser pulse. The average transverse velocity of the electron due to the gradient force is

$$\langle v \rangle = \frac{\Delta P_T}{2\gamma m},$$

on recalling a result of section 2-2d of ref. 1 that the energy of the electron inside the wave field is approximately γmc^2 so long as $\eta_0 \ll \gamma$.

The electron moves transversely by $\langle v \rangle z_R/c$ on its way into the pulse. We require this to be much less than σ_r , otherwise the electron will be deflected out of the core of the beam. Thus we arrive at the condition

$$\frac{\eta_0^2}{\sqrt{1+\eta_0^2}} \ll \frac{\gamma\lambda^2}{4\pi^2\sigma_r^2} = \frac{\gamma}{4(f/d)^2}.$$

In the proposed experiment to demonstrate the nonlinear effects of large η on Compton scattering, a value of $\eta_0 \approx 0.3$ is perhaps optimal. For smaller η the effects are very small, and for larger η the various multiphoton contributions blur into a continuum. Hence we need

$$\gamma \gg 0.4(f/d)^2 = 1.6,$$

if we use a lens with $f/d = 2$. As $\gamma = 100$ for 50-MeV electrons, there should be little problem of the electrons being diverted from the core of the laser pulse.

Appendix B. Attenuation of the Electron Beam by Compton Scattering

The electrons may suffer a Compton scatter before they reach the center of the laser pulse, and hence the signature of any nonlinear QED effects at the pulse center would be confused.

We return to an argument given in section 2-2c of ref. 1.

For pulses with $\eta_0 \lesssim 1$ we may use the Larmor formula for the rate of energy loss by an electron to Compton scattering (if the center-of-mass energy is so high that quantum corrections are important, these always reduce the rate!):

$$\frac{dU^*}{dt^*} = \frac{2e^4 E^{*2}}{3m^2 c^3},$$

where the superscript \star indicates quantities to be evaluated in the (average) rest frame of the initial electron. It is memorable to use one cycle of the laser field oscillation as the unit of time: $dt^\star = 2\pi/\omega^\star$. Then the energy radiated in one cycle of the wave is

$$dU^\star = \frac{4\pi e^4 E^{\star 2}}{3m^2 c^3 \omega^\star} \text{ per cycle.}$$

The number of photons radiated is

$$dN = \frac{dU^\star}{\hbar\omega^\star} = \frac{4\pi e^2}{3} \frac{e^2 E^{\star 2}}{\hbar c m^2 \omega^{\star 2} c^2} = \frac{4\pi}{3} \alpha \eta_0^2 \text{ photons per cycle.}$$

The effective number of cycles during which this radiation occurs (as the electron enters the laser pulse) can be estimated as the Rayleigh range divided by the wavelength:

$$\frac{z_R}{\lambda} = \frac{4\pi\sigma_r^2}{\lambda^2} = \frac{4}{\pi} \left(\frac{f}{d}\right)^2,$$

supposing the laser is focused in a lens of focal length f and aperture d as described in Appendix A. Again we note that this is a short time compared to the temporal pulse length of any laser that might be used for high-field studies.

Then the number of photons radiated per electron as the electron enters the laser pulse is

$$dN = \frac{16}{3} \alpha \left(\frac{f}{d}\right)^2 \eta_0^2 \approx 0.04 \left(\frac{f}{d}\right)^2 \eta_0^2 \approx 2.3P[\text{TeraWatts}].$$

A good lens might have $f/d = 2$, for which there would be only a 16% chance of an electron undergoing a Compton scatter on the way into a laser beam with $\eta_0 = 1$. And for $\eta_0 < 1$, the scattering rate is quadratic in η_0 .

Thus even when a single Compton scatter effectively removes the electron from the beam, studies of nonlinear effects should be possible for laser field with η_0 of order 1.

For the proposed experiment at $U = 50$ MeV, the electron loses at most 4.7 keV in a Compton scatter, and for $\eta_0 = 0.3$ the average number of Compton scatters per electron on the way into the laser pulse is 0.018 according to the present estimate. The total scattering rate is then estimated to be 0.036, which compares well with the value of 0.05 calculated in a detailed analysis as discussed in Section 2.

In any case, the Compton scatter could be important only if the electron loses a significant fraction of its energy in the scatter. Now the maximum energy lost by an electron that Compton scatters in a wave field with $\eta_0 \ll 1$ is

$$\frac{\Delta U}{U} = \frac{4\gamma\omega/m}{1 + 4\gamma\omega/m},$$

where ω is the energy of a photon of the wave field. Hence the possible attenuation of the electron will be important only for

$$\gamma \gtrsim \frac{m}{4\omega}.$$

However, this includes the interesting case that $U = 50$ GeV (SLAC or LEP) for which $\gamma = 10^5$ and $\omega = 1$ eV as for a Nd:YAG laser.

A future interest in nonlinear QED with a 50-GeV electron beam involves studies of light-by-light scattering. Here the electron-laser collision serves only to produce a high-energy photon beam that is then scattered against a second piece of the laser pulse. [Both scattered and unscattered electrons are swept away before the light-by-light collision.] It is desirable for this that the probability of a Compton scatter of a 50-GeV electron be near one, for which we need only $\eta_0 \approx 1$ as noted above.

In principle, the high-energy photon beam might be attenuated by interaction with the leading edge of the laser pulse via the Breit-Wheeler process

$$\gamma\gamma \rightarrow e^+e^-,$$

whose cross section is similar to that for Compton scattering. However, we are actually below the kinematic threshold for this process if we use 50-GeV electrons and a YAG laser; it can only occur via multiple laser photons. Thus the high-energy photons will not interact at all with the laser until they reach the core of the laser beam where $\eta \approx 1$.

As a final remark, we consider the possibility of vacuum Čerenkov radiation, in which an electron emits a Čerenkov photon in the vacuum as polarized by a strong wave field. The threshold electron energy for this effect is given by

$$\gamma_0 = \frac{m}{\eta_0\omega} \sqrt{\frac{1 + \eta_0^2}{22\alpha/45\pi}}.$$

To keep the Čerenkov threshold ‘low’ it is desirable to operate the laser near $\eta_0 = 1$, but it does not pay to go much higher as the threshold changes little once $\eta_0 > 1$. Again, the attenuation of the electron beam by Compton scattering with the laser would be annoying but not fatal for such an experiment.

Appendix C. Anomalous Compton Scattering

The nonlinear Compton scattering reaction may be written as

$$e + l\omega \rightarrow e' + \omega',$$

in which l laser photons of frequency ω are absorbed by an electron, which then radiates a single photon of frequency ω' .

If the collisions between the electron and the laser beam occur in a medium with an index of refraction n , and $\beta > 1/n$, then so-called anomalous Compton scattering becomes possible:

$$e \rightarrow e' + l\omega + \omega'.$$

Here the incident electron radiates l photons into the laser beam, along with another photon of frequency ω' that could be detected. If $l = 0$, we have ordinary Čerenkov radiation; for $l > 0$ we have a curious combination of Compton scattering

and Čerenkov radiation. This effect has been considered theoretically by Becker¹³ (see also Kroll¹⁴).

The kinematics of anomalous Compton scattering are readily derived; one should allow for dispersion of the index and define n' as the value of the index at the frequency ω' . Then for $l > 0$

$$\omega' = \frac{l\omega(1 + n\beta)}{n'\beta \cos \theta - 1}.$$

We see that ω' is defined only for

$$\cos \theta > \cos \theta_C = \frac{1}{n'\beta}.$$

That is, the anomalous Čerenkov radiation can only occur inside the Čerenkov cone.

A calculation¹² of the intensity I_1 of the anomalous Compton scattering for the case $l = 1$ shows that it can be related to the intensity I_0 of Čerenkov radiation by

$$I_1 = \frac{\eta_0^2 I_0}{2\gamma^2 \beta^2 (1 + n\beta)}.$$

Thus in principle the anomalous Compton scattering could become prominent if we can attain $\eta_0 \sim 1$ in a medium of index n .

However, a laser pulse of $\eta_0 \sim 1$ would convert any material into a plasma and the index of refraction would be a transient. For a CO₂ laser it may be possible to transmit an intensity of 100 GW into a NaCl crystal without damage (P. Corkum, private communication). If so, we could achieve $\eta_0^2 \sim 4 \times 10^{-6}$, according to the expression p. 2. Then with a 50-MeV electron beam we might have $I_1 \sim 10^{-10} \cdot I_0$. This is rather daunting, but we could use a bunch of 10^9 electrons as a tight focus is not required.

The Čerenkov radiation rate can (per cm per electron) be written

$$I_0 = \frac{2\pi\alpha}{\lambda} \sin^2 \theta_C \frac{\Delta\omega'}{\omega'}.$$

On examining the kinematics of anomalous Compton scattering for the case of a NaCl crystal of index ~ 1.5 - 1.6 , we find that $\lambda \sim 0.75 \mu\text{m}$, and that if this light is collected in a 30° cone about the electron-beam direction then $\Delta\omega'/\omega' \sim 0.25$. For NaCl, $\sin^2 \theta_C \sim 0.5$. Combining the various factors, we estimate about 10^{-7} anomalous Compton scatters per electron crossing a 1-cm-thick plate of NaCl. With 10^9 electrons per bunch there would then be about 100 such photons per ATF pulse.

The interaction region for the nonlinear Compton scattering experiment could readily be modified to accommodate the observation of anomalous Compton scattering. A detector for $0.75\text{-}\mu\text{m}$ photons would be required. We will examine this possibility in more detail in the coming months.

Appendix D. Interference in Nonlinear Compton Scattering with Two Laser Beams

An interesting interference effect involving nonlinear Compton scattering has been pointed out by Puntajer and Leubner.¹⁵ Suppose an electron collides with two co-propagating laser beams, one at twice the frequency of the other (as results from use of a frequency-doubling crystal). Then second-harmonic scattering from the lower-frequency laser is indistinguishable from first-harmonic scattering from the higher-frequency laser. Hence there will be an interference effect, which leads to an up-down asymmetry of the scattering in the plane of the (linear) laser polarization. Note that the interference effect involves three laser photons.

The (classical) calculational technique used by Puntajer and Leubner appears inadequate for the case of relativistic electrons or laser intensities with $\eta \sim 1$, but we anticipate that this can be remedied by a more careful approach such as that of Sarachik and Schappert.¹⁶

The experiment could be readily performed at the ATF with the addition of a Nd:YAG or Nd:glass amplifier capable of producing 10–100-gigaWatt pulses. It would be favorable to reduce the electron-beam energy to 35 MeV so that the second-harmonic x-ray energy would be only 50 keV.

References

1. K.T. McDonald, ‘Proposal for Experimental Studies of Nonlinear Quantum Electrodynamics,’ DOE/ER/3072-38, Princeton University (Sept. 1986).
2. G.A. Schott, *Electromagnetic Radiation*, (Cambridge University Press, 1912).
3. For a textbook discussion, see V.B. Berestetskii *et al.*, *Quantum Electrodynamics*, (Pergamon Press, 1982), §101, p. 449.
4. T.J. Englert and E.A. Rinehart, ‘Second-Harmonic Photons from the Interaction of Free Electrons with Intense Laser Radiation,’ *Phys. Rev. A* **28**, 1539 (1983).
5. J. Fisher, T. Srinivasan-Rao and T. Tsang, ‘UV Photoemission from Metal Cathodes for Picosecond Power Switches,’ in *Proceedings of the Switched Power Workshop* (Shelter Island, Oct. 1988).
6. W. Chen *et al.*, ‘Proposal for a Study of Laser Acceleration of Electrons Using Micrograting Structures at the ATF,’ (Oct. 1989).
7. T. Shimada *et al.*, ‘Generation of High-Brightness 1.06 μm Pulses by compression of a Chirped Seed in a Nd:YAG Regenerative Amplifier,’ Los Alamos preprint LAUR-88-3742, contributed to the Conference on Lasers and Electro-Optics 89 (Baltimore, 1989).
8. T. Shimada *et al.*, ‘Large-Volume High-Pressure CO₂ Laser for Ultrashort Pulse Amplification,’ Los Alamos preprint LAUR-87-3766, contributed to the Conference on Lasers and Electro-Optics 88 (Anaheim, 1988).
9. M.J.W. Rodwell *et al.*, ‘Subpicosecond Laser Timing Stabilization,’ *IEEE J.Q.E.* **25**, 817 (1989).

10. P.B. Corkum, 'Amplification of Picosecond 10- μ m Pulses in Multiatmosphere CO₂ Lasers,' IEEE J. QE-**21**, 216 (1985).
11. D.P. Russell and K.T. McDonald, 'A Beam-Profile Monitor for the BNL Accelerator Test Facility,' to appear in the Proceedings of the 1989 Particle Accelerator Conference (Chicago, March, 1989).
12. R.W. Gould *et al.*, 'Application of the Graphite Monochromator to Light-Element X-Ray Spectroscopy,' Appl. Spectr. **22**, 549 (1968); C.J. Sparks, Jr., 'Mosaic Crystals for Obtaining Larger Energy Bands and High Intensities from Synchrotron Radiation Sources,' in *Workshop on X-Ray Instrumentation for Synchrotron Radiation Research*, ed. by H. Winick and G. Brown (SSRL Report 78/04, Stanford, 1978), p. III-35.
13. W. Becker, 'What is Left from Stimulated Electromagnetic Shock Radiation. A Quantum Approach,' Phys. Rev. A **23**, 2381 (1981).
14. N.M. Kroll, 'Relativistic Synchrotron Radiation in a Medium and Its Implication for SESR,' in *Free Electron Generators of Coherent Radiation*, ed. by S.F. Jacobs *et al.* (Addison Wesley, 1980).
15. A.K. Puntajer and C. Leubner, 'Asymmetries in Intense Laser – Free Electron Scattering,' U. Innsbruck (1988).
16. E.S. Sarachik and G.T. Schappert, 'Classical Theory of the Scattering of Intense Laser Radiation by Free Electrons,' Phys. Rev. D **1**, 2738 (1970).